2016

Fabrication and Investigation of an enzyme-free, Nanoparticle-based Biosensor for Hydrogen Peroxide determination

Craig Neal
University of Central Florida

FABRICATION AND INVESTIGATION OF AN ENZYME-FREE, NANOPARTICLE-BASED BIOSENSOR FOR HYDROGEN PEROXIDE DETERMINATION

by

CRAIG JAMES NEAL
B.S. University of Central Florida, 2014

A thesis submitted in partial fulfillment of the requirements
for the degree of Master of Science
in the Department of Material Science and Engineering
in the College of Engineering and Computer Science
at the University of Central Florida
Orlando, Florida

Summer Term
2016

Major Professor: Sudipta Seal

ABSTRACT

Electrochemical biosensors often employ enzymes as detection elements. These sensors are highly selective towards target analytes, however the scope of their application is limited by the poor stability of the enzyme. In this study, multi-valent inorganic cerium oxide nanoparticles were used as detection elements for the analysis of hydrogen peroxide. The electrochemical response of the cerium oxide towards hydrogen peroxide analyte is defined through cyclic voltammetry and chronoamperometry. This response was found to be dependent on nanoparticle Ce3+:Ce4+ redox state ratio and this property is exploited to fabricate a biosensor. As produced, the biosensor demonstrated sensitivity at picomolar analyte concentrations. Further, the sensitivity of the electrode is stable across a range of temperatures and pH's which inhibit the function of standard enzyme-based sensors. Additionally, the produced sensor retained function in sheep serum demonstrating the high selectivity and robustness of the sensor.

This work is dedicated to my parents for their constant support and motivation.

ACKNOWLEDGMENTS

Would like to acknowledge the efforts of Shashank Saraf, Swetha Barkam, Soumen Das, and Ankur Gupta. I would also like to extend kind thanks to Dr. Sudipta Seal for his advisory throughout this research and to Dr. Hyoung Jin Cho for his guidance and insight. Funding of this research and graduate student support was possible through several contracts and grants to Dr. Seal.

TABLE OF CONTENTS

ABSTRACT iii

ACKNOWLEDGMENTS v

TABLE OF CONTENTS vii

LIST OF FIGURES viii

CHAPTER ONE: INTRODUCTION 1

CHAPTER TWO: METHODOLOGY 6

2.1 Materials 6

2.2 Methods 6

2.2.1 Particle Synthesis & Characterization 6

2.2.2 Biosensor Fabrication 7

2.2.3 Electrochemical Testing 9

CHAPTER THREE: RESULTS AND DISCUSSION 13

CHAPTER FOUR: CONCLUSION 32

LIST OF REFERENCES 34

LIST OF FIGURES

Figure 1 SEM image of Porous, Glassy Carbon electrode surface. The observed pore structure occurs to the degradation of PAN acryl groups. The formed species are volatile and are released from the material during processing. The size of the observed pores has a bi-modal distribution with average pore sizes around ~500 and 850nm; ostensibly, facilitating the retention of CNPs on the electrode for the fabricated sensor device platform. 8

Figure 2 Clean gold cyclic voltammagram in H_2SO_4. The peak at ~0.8V was used to quantify the electro-active gold surface area. This peak is particular to the reduction of surface gold atoms and, therefore, integrating this peak will give a normalizable value for the electro-chemically active (oxidizable) gold at the surface. 10

Figure 3 CNP (Left to Right, CNP1,2,3) size Characterization (TEM images) with insets illustrating crystallinity (all scale bars are 20 nm). All formulations show aggregation due to the high reactivity of NP surfaces. Images show well-formed, individual crystallites. Further, these images highlight the crystallinity of these particles through the clear presence of lattice fringes... 14

Figure 4 Diagrammatic representation of CNP collision at gold macro-electrode. Collision allows for reduction of adsorbed peroxy species at the working electrode surface and for the re-formation of the ceria surface oxygen vacancies. 15

Figure 5 (a) Catalase Assay. Activity was greatest for CNP1 followed in descending order of activity by CNP2 and 3. (b) CV for all CNP preparations (1 mM H_2O_2 and CNPs), cathodic peak

current (inset). The inverse relationship between Ce3+:Ce4+ ratio and catalase activity holds for CV. Additionally, an anodic peak present for all formulations shows a positive relationship between Ce^{3+}:Ce^{4+} ratio and current. 16

Figure 6 Current Dependence on Scan Rate for CNP-Hydrogen Peroxide reaction at Reduction peak. Linear fitting of the peak reduction current vs. the inverse of scan rate produces an R^2 value of 0.99. This is evidence that the CNP-H_2O_2 reaction is diffusion limited at -0.23V. 19

Figure 7 Concentration dependence and peaks character for CNP 1 and 2 formulations. Peaks 1 and 2 show a concentration dependent current response towards hydrogen peroxide. Additionally, the peak at ~0.8V becomes broader- moving towards lower potential values; suggesting a more complex redox mechanism at the electrode. 20

Figure 8 (a) Picomolar detection by Biosensor. Addition of H2O2 to a final concentration of 1pM produces a 350nA signal, compared with the nanomolar limit of detection of most enzymes. (b) Nano v. Micro particle characterization. CNPs show significantly greater sensitivity towards H2O2 analyte as compared to ceria microparticles-based sensor; this greater signal is attributed to nano-size effects and specifically to the change in nanomaterial surface chemistry/physics. . 21

Figure 9 CNP3 CA with addition of Competitive species and H_2O_2. Competitive species addition causes no significant change in current. H_2O_2 addition causes immediate response with each addition. 22

Figure 10 1mM Glucose in dH_2O cyclic voltammogram. Glucose control was run to determine redox interaction with gold. Glucose produces a current response however, the response is not concentration dependent. Therefore, presence of glucose can be disregarded as a background

current signal and changes to glucose concentration will not interfere with the sensors current response to hydrogen peroxide analyte. 23

Figure 11 Cyclic voltammagram of Sodium Nitrite in water at 10uM and 1mM. The voltammagram shows little change in current response with concentration of analyte at our determined sensor operating potential, -0.23V. 24

Figure 12 Uric Acid Cyclic Voltammetry interfering species. Voltammetry at 1 and 0.01mM concentrations shows little change in current at the hydrogen peroxide reduction potential. From this, it seems that the sensor will operate independent of uric acid concentration and that presence of uric acid will only contribute to background current. 25

Figure 13 CA (i) of CNPs1 **(a)** & 3 **(b)** in solution with regression for each **(ii)**. **(ai & bi).** Measurements for both formulations show good linear fit between current and H_2O_2. Comparison between these two responses corroborates results in CV measurements and allows for optimization of the CNP sensing element in biosensor application. 27

Figure 14 Diagrammatic representation of deposited CNP film on glassy carbon substrate. Particles are located directly on the electrode surface allowing for immediate peroxy species reduction and for high electron flux due to the fixed position of the CNPs at the electrode surface. 28

Figure 15 Sensor detection range for H2O2. The detection range is across eight orders of magnitude from 0.1pM to 0.1uM. 29

Figure 16 The sensor shows no loss in activity from (a) pH 4.0 to 8.0 or from (b) 20 to 40^0C , as compared with HRP which loses significant activity across these ranges. Further, experiences a

melting point at 42^0C resulting in loss of tertiary structure. (c) CA with nafion-coated CNP-based sensor in blood serum. Serial additions of 1uM H2O2 produces clear current signal suggesting absence of bio-fouling. 30

LIST OF TABLES

Table 1 Ceria Nanoparticle properties 13

CHAPTER ONE: INTRODUCTION

The field of sensor technology is ever-improving with sensors developed for applications requiring high sensitivity, high selectivity, and fast response times. Herein, bio-sensing devices represent a significant portion of devices for bio-sensing have seen an especially pronounced growth. Within the biomedical field and numerous other industries, hydrogen peroxide is an analyte of significant importance.

Within industrial settings, hydrogen peroxide (H_2O_2) is a critically important analyte. These industries vary widely spanning from manufacturing to food production to pharmaceuticals and medicine. High precision measurements are especially important for quantifying H_2O_2 in processes for endpoint products used directly by consumers; for example, in food sterilization, pharmaceuticals production, and medical devices.

H_2O_2 detection has been accomplished primarily through titration [(Reichert et al. 1939)], UV-Vis spectroscopy [(Nogueira et al. 2005)], fluorescence [(Gomes et al. 2005)], chemiluminescence [(Hanaoka et al. 2001)], and electrochemical methods. The majority of these techniques rely on optical detection. These techniques will, by their nature, be more costly through acquisition/upkeep of instruments. In contrast, electrochemical methods require only limited instrumentation while providing high precision data over short time periods. Additionally, detection can be performed through analyte oxidation or reduction: allowing for application of a greater range of chemical systems. Further, electrochemical methods can be performed to monitor changes in current (amperometric), voltage (voltammetric), or impedance (electrochemical impedance). When greater levels of precision are

required, these methods can be coupled with optical techniques (i.e. photoelectrochemical methods and electrochemical luminescence): producing detection methods with significantly greater precision than either set of techniques individually. Previously, application of electrochemical methods for the detection of H_2O_2 have been limited by the over-potential necessary for oxidation/reduction and by the slow kinetics of electron transfer [(Chen et al. 2012)]. In recent works, chemically modified electrodes have been employed to successfully remove these limitations. Specifically, these modifications have entailed functionalizing the electrode surface with polymers, bio-molecules, redox-active small molecules, enzymes, and nanomaterials [(Chen et al. 2012), (Zhao et al. 2011),(Chen et al. 2012)]. Use of these species allows the electrode to be sensitized to particular analytes: making redox more efficient. In this way, electrodes can be fabricated for use as sensor devices. Small molecules and nanomaterials are thoroughly represented in the literature of electrochemical sensors. However, enzymes are utilized the most over other functional materials, as sensing elements for electrochemical biosensors.

Enzymes are bio-molecules which catalyze chemical reactions necessary for life in an organism. These molecules have been developed and modified through gene transfer and selection through generations of organisms to have high catalytic efficiency. This perpetual refinement has made enzymes highly selective and sensitive towards certain chemical substrates with turnover rates fast enough to support life processes. These qualities have been translated to biosensors by utilizing enzymes as sensing elements for chemical species of physiological importance. However, use of these molecules is not without drawbacks. By their nature, enzymes are designed to be extremely sensitive to particular physical and chemical conditions. This is to ensure that metabolism remains localized to particular body regions (e.g. metabolism necessary for one tissue

may have a completely adverse effect in another; further, some metabolic products function as signaling molecules for activation of highly tissue-specific responses). Small variance from native conditions in pH, ionic strength, temperature, or light exposure can produce substantial, in some cases irreversible, loss of activity. For H_2O_2 detection specifically, the enzyme horseradish peroxidase (HRP) is used most frequently [(Xu et al. 2004), (Delvaux et al. 2004), (Long et al. 2008)]. This enzyme is not only common to biosensors, but has seen extensive use throughout biomedical sciences. However, as with any protein, HRP is highly susceptible to storage/operation conditions. The protein loses activity with pH changes from 8 to 4 (- >60%) and from 40 to 20^{o}C (- 30%) when immobilized on an inert substrate [(Temoçin and Yiğitoğlu 2008)]. These changes in activity were attributed to partial loss in the tertiary structure which expose the enzyme's active site to solution molecules. Exposure of the active site decreases the favorability of the catalyzed chemical reaction resulting in decreased enzyme activity. For HRP, complete, irreversible loss of activity occurs at 42^{o}C [(Chattopadhyay and Mazumdar 2000)]. Due to the inherent shortcomings of enzyme-based detection, researchers are moving more into the use of enzyme-free sensors (using sensing elements of the types detailed above). In most cases, detection is achieved through incorporation of inorganic nanoparticles or coatings [(Wang 2006), (Qu et al. 2007),(You et al. 2011)].

Cerium oxide (ceria) has seen extensive use in myriad applications as a functional material spanning from medical devices to chemical catalysis to semiconductor processing and nearly every other corner of science and technology. Specifically, ceria has seen use in oxygen sensors, in capacitive devices, as a polish material in semiconductor fabrication, in sold oxide fuel cells, and in self-cleaning ovens. The utility of ceria comes from its ability to interconvert between Ce^{3+} and Ce^{4+} redox states in presence of particular oxygen-containing-species and to release/store oxygen

by the formation/loss of oxygen vacancies in the crystal lattice. Cerium oxide (Ceria) has also demonstrated significant, biomimetic reactivity towards reactive oxygen and nitrogen species. [(Asati et al. 2009),(Dowding et al. 2013),(Korsvik et al. 2007),(Pirmohamed et al. 2010),(Dowding et al. 2012)]. Specifically, hydrogen peroxide, superoxide anion, hydroxyl anion, peroxy nitrite have been assessed. Reflecting this, use of ceria as a therapeutic agent in diseases such as cancers, neurodegenerative diseases, and ophthalmological diseases have shown great promise for potential clinical application [(McGinnis et al. 2010),(Walkey et al. 2015),(Self et al. 2016),(Dowding et al. 2014),(Sack et al. 2014),(Jana et al. 2014),(Cai et al. 2014),(Alili et al. 2011),(Wason et al. 2013),(Das et al. 2013)]. Ceria's enzymatic activity is specific to the ratio of Ce^{3+} to Ce^{4+} in the material and is due to redox between these states. Further, this modification of this ratio will make the material more or less sensitive towards individual analytes. Additionally, as the dimensions of the ceria lattice are decreased to the nano-scale, the prevalence of Ce^{3+} increases along with the number of oxygen vacancies due to an increase in bond strain [(Deshpande et al. 2005a)]. This material property is especially important for surface catalyzed chemical reactions, wherein the increased energy from bond strain and the presence of oxygen vacancies makes reaction more favorable. Chemical species containing oxygen groups react with ceria surface oxygen vacancies, producing a redox change and removing the vacancy. Therefore, ceria nanomaterials show unique activity and reactivity [(Gupta et al. 2016), (Tarnuzzer et al. 2005),(Korsvik et al. 2007),(Heckert et al. 2008)]. Several studies have been produced which use ceria nanoparticles (CNPs) as sensing elements for hydrogen peroxide [(Ansari et al. 2008; Saha et al. 2009), (Seal et al. 2012)]. In most cases these devices incorporate an enzyme for detecting an analtye of interest while a layer of ceria is used to detect a hydrogen peroxide metabolic product from the enzyme interaction; specifically, cholesterol oxidase, and glucose oxidase have been tested. These studies are limited to vary narrow operation conditions due to

these enzymes, as detailed above. Further, these studies do not demonstrate high sensitivities.

In the present study, different preparations of CNPs are used to determine whether the ratio of Ce^{3+}:Ce^{4+} has a direct relationship with the electrochemical response. Then, the determined relationship is used to develop a biosensor platform optimized for electrochemical response to hydrogen peroxide.

CHAPTER TWO: METHODOLOGY

2.1 Materials

Nano-pure diamond distilled water; 30% NH_4OH, 30% Hydrogen Peroxide, Cerium nitrate hexa-hydrate (trace metals basis, 99.999%), 1% nafion, poly(acrylonitrile), sodium phosphate dihydrate, sodium diphosphate monohydrate, sodium acetate, hydrogen chloride, and sheep's blood serum from Sigma Aldrich; Cerium Oxide nanoparticles 20% colloidal suspension in water from Alfa-Aesar; powder cerium oxide microparticles from REaction a John Mathis company

2.2 Methods

2.2.1 Particle Synthesis & Characterization

For this study, three different, previously studied/characterized CNP synthesis methods were employed to produce particles with different Ce^{3+}:Ce^{4+} ratios.

CNP1: Dissolved cerium nitrate hexahydrate in 20mL of dH_2O. Subsequently, a stoichiometric amount of 30% H_2O_2 was added.

CNP2: Alfa-Aesar CNPs were diluted from purchased stock bottle using dH_2O (> 18MOhms), as required for given measurements. No further procedure was performed on these particles (solely dilution).

CNP3: Forced hydrolysis synthesized CNPs through NH_4OH-mediated precipitation. Then, the solution was centrifuged at 8000rpm to collect the as-formed particles. These particles

were re-dispersed into colloidal suspension by adding to dH_2O and titrating the solution to a pH of ~4 using nitric acid.

All CNPs were characterized using x-ray photoelectron spectroscopy (XPS) (Physical Electronics (PHI5400 ESCA) spectrometer with a monochromatic Al Kα X-ray source at 300W with a base pressure of 5x10^(-8) Torr) to determine the relative amounts of 3^+ and 4^+ ceria redox states. UV-Vis spectroscopy was conducted at 1mM concentrations. TEM (Phillips FEI Tecnai F30 at 3000keV) imaging was performed to visualize the particles. These images allowed interpretation of particle size, shape, dispersity, and crystallinity.

2.2.2 Biosensor Fabrication

Si wafers (with natural oxide layer intact) were cut to ~ 1x1cm squares; then, the wafers were cleaned through ultra-sonication in acetone→ethanol→ then water. Lastly, the cut silicon was dried under nitrogen.

The glassy carbon thin film electrodes were produced through poly(acrylonitrile) (PAN) polymer decomposition. 150kDa PAN was first dissolved in dimethylformamide (8wt%) at 40° C with this temperature then being held for 30 minutes. The dissolved polymer was then spin-coated on Si wafer as part of a two step process. Initially, 50μL of the solution was dropcast at 2000rpm for 1 min. Following this, the spin-coating speed was raised to 3000rpm for half a minute to produce an even thickness for the polymer coating. The as detailed wafers were subsequently held at 250° C for an 1hr. Carbonization was then performed in a furnace in an inert atmosphere (Ar; flow rate: 150mL/min). Samples were heated to 900° C at a constant rate of 5C° /min and held in these conditions for an hour. The samples were cooled to room temperature at a rate of 5C° /min.

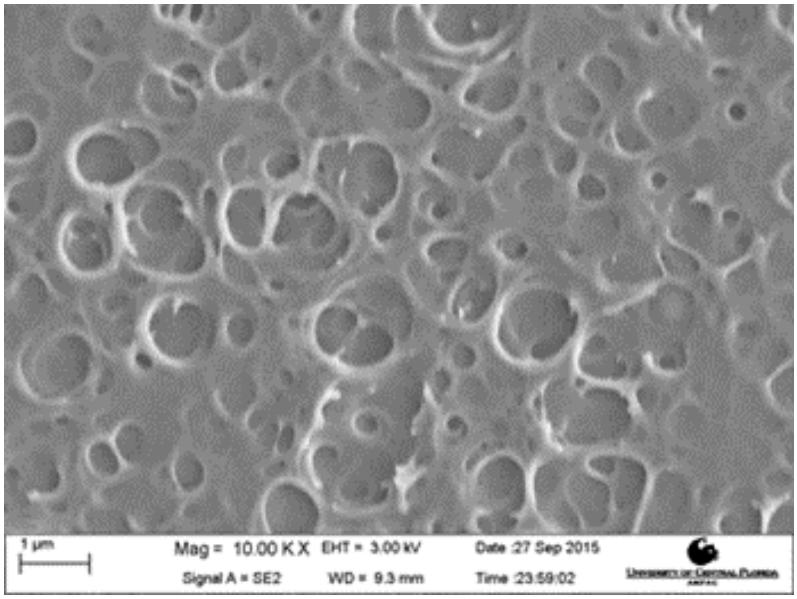

Figure 1 SEM image of Porous, Glassy Carbon electrode surface. The observed pore structure occurs to the degradation of PAN acryl groups. The formed species are volatile and are released from the material during processing. The size of the observed pores has a bi-modal distribution with average pore sizes around ~500 and 850nm; ostensibly, facilitating the retention of CNPs on the electrode for the fabricated sensor device platform.

Glassy carbon electrode substrates were next brought to ~300 C and 200uL of a CNP formulation/suspension was drop-cast from a 0.2mM stock solution of CNP3. The substrates were then held at this temperature (300^{o}C), for 3 hours, in air. Following this time period, the electrodes were slowly (to avoid cracking of the deposited CNP layer on the electrode surface) allowed to cool within the furnace.

Device electrical contacts were made using a silver paste and a polished copper wire and was done before addition of CNPs (so that contacts were formed on the conductive glassy carbon surface). After heating, the paste becomes dry and brittle. This layer was subsequently dissolved

using acetone and a fresh layer of silver paste was added to the CNP-free electrode surface (over the original paste position. Following this, the electrodes were rinsed with de-ionized water and allowed to dry under vacuum. When not in use, the electrodes were stored at room temperature in translucent, plastic boxes.

For experiments entailing measurements in blood serum, the electrodes were further coated with a thin layer of nafion polymer (10uL of 0.01% in water) and allowed to dry overnight under vacuum to prevent protein adsorption to the CNP layer during testing in serum.

2.2.3 Electrochemical Testing

Electrical potentials for all measurements were referenced against Ag/AgCl reference electrodes (3M KCl storage and fill solutions). Prior to running any experiments, platinum-mesh counter electrodes were cleaned by an electrochemical process in a 0.5M H_2SO_4 solution through cyclic voltammetry (CV). The chosen potential range was from 1.6 to -0.5V and was conducted for 50 cycles at 1V/s. Electrodes were determined to be clean once subsequent voltammagrams showed little variation in current intensity and peak structure/distribution. Round-disk gold working electrodes (CH instruments) were cleaned by the same protocol, however, they were first polished using an aluminum slurry (0.5micron particles). Additionally for gold, the potential range was swept between 1.2 and -0.4V. Any time an electrode was polished via slurry, electrochemical cleaning was subsequently performed; this is due to the possibility of surface contamination by the oil based slurry which has been shown in other studies to dramatically alter CV measures. The intensity of the gold reduction peak (~0.8 V in CV) was used to represent the electro-active surface area of the working electrode: allowing for normalization of current values across measurements (since the gold surface may be electrochemically de-activated by surface contamination or

experience topological changes from etching/roughening). Measured current was then converted to current density using the electrochemically active surface area for comparison across multiple measurements. Figure 2 is a cyclic voltammagram representative of a clean gold electrode in sulfuric acid used for electrode cleaning.

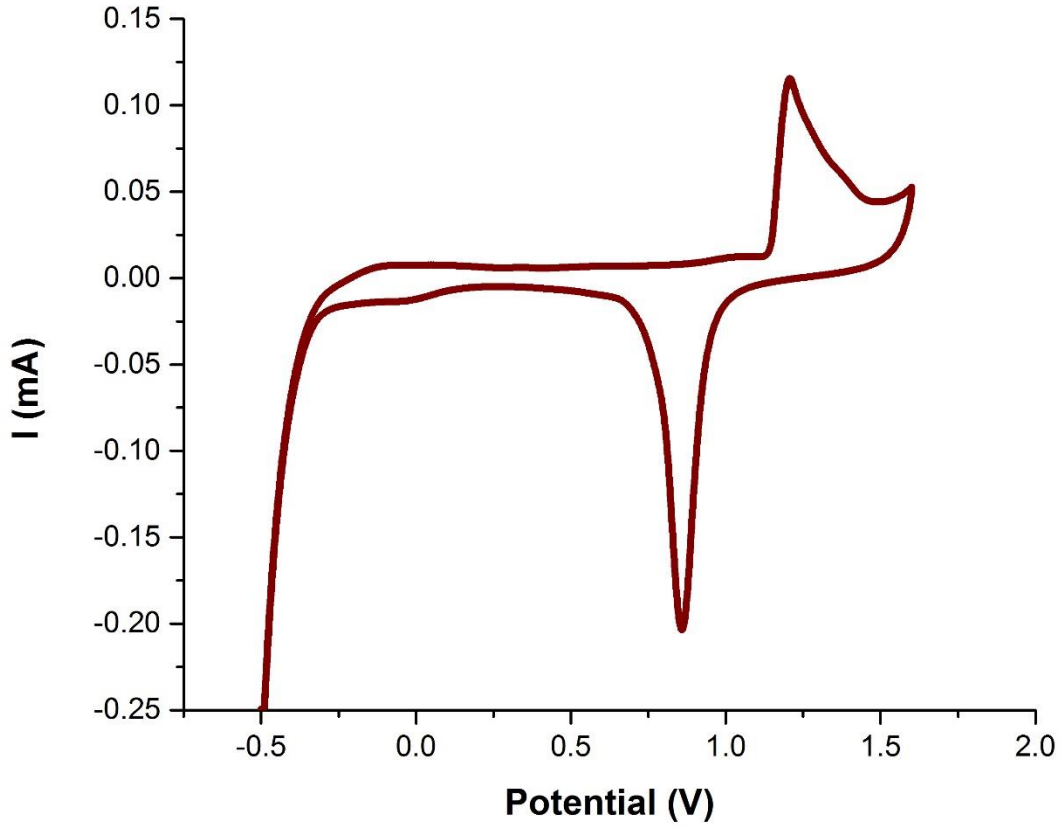

Figure 2 Clean gold cyclic voltammagram in H_2SO_4. The peak at ~0.8V was used to quantify the electro-active gold surface area. This peak is particular to the reduction of surface gold atoms and, therefore, integrating this peak will give a normalizable value for the electro-chemically active (oxidizable) gold at the surface.

These initial CV measurements with CNPs suspended in solution involve the collision of the nanoparticles with the electrode surface. Generally, these collision-mediated measurements are performed using microelectrodes to record individual particle collisions (allowing for the characterization of nanoparticle composition, shape, and/or size). In the present study, characterization of particle electrochemical activity of similar size, shape, and zeta potential particles was desired. Therefore, large magnitude particle flux at the electrode-solution interface is ideal; was accomplished using a macro- working electrode for all measurements. As a result of this, in chronoamperometric measurements, a staircase/stepped current response was observed. This response is compared with the spiked current graphs characteristic of low concentration nanoparticles at the surface of a micro- working electrode (the stepped response being related to the comparatively high particle flux at the working electrode surface due to the high particle concentration) [(Allen J. Bard 2001),(Rees et al. 2012)]. CV was conducted with 1mM CNPs (for each of the three different CNP formulations) dispersed in 10mL of dH_2O and a potential range from 0.8V to -0.3V with a scan rate of 20mV/s. H_2O_2 was added at 0.01, 0.1, 1, 2.5, and 5mM concentrations and measurements were repeated five times at each concentration. Electrodes were cleaned as detailed above prior to and between any measurement. CV was performed on control solutions without CNPs to determine the influence of any other solution components on electrochemical measures. Chronoamperometry (CA) was performed using a potential bias of -0.23V, based on the redox activity seen in cyclic voltammagrams, with 1mM solutions of CNP formulations 1 and 3. Prior to any given measurement, the electrochemical response was allowed to equilibrate over a period of 30 seconds. Then, current changes were recorded over 10 minutes with addition of analytes by pipette in 100uL volume increments. Following this, CNP- or ceria

microparticle (CMP)-based sensors were tested under identical experimental conditions, without interfering species, to assess the implications of nanoscale material properties as they relate to the observed electrochemical response. The fabricated biosensor was evaluated through chronoamperometry performed at the same voltage as used for CNPs in solution. H_2O_2 addition was done in 100uL increments after a 30 second equilibration period in either 100mM $NaNO_3$ or sheep's blood serum.

CHAPTER THREE: RESULTS AND DISCUSSION

In the presented study, three different CNP formulations were produced through different synthesis methods. The synthesis procedure for each of these methods were used from previous studies wherein, particle characterization showed differing ratios of Ce^{3+} and Ce^{4+}. X-ray photoelectron spectroscopy (XPS) was performed for each of these to confirm differences in Ce^{3+}:Ce^{4+} ratio (Table 1). This ratio was found to decrease across the formulations from CNP1→3. Before comparing the electrochemical activity of the varied Ce^{3+}:Ce^{4+} formulations, it was necessary to characterize certain physicochemical properties for each; namely: particle size, morphology, and zeta potential, (collected in Table 1).

Table 1 Ceria Nanoparticle properties

	Morphology	Size (nm)	Zeta Potential (mV)	Ce^{3+}:Ce^{4+} (XPS)
CNP1	Spherical	3-5	4.571	1.06
CNP2	Spherical	3-5	3.245	0.39
CNP3	Spherical	3-5	1.336	0.24

Particle size and morphology (TEM imaging) were similar for all formulations. TEM micrographs (Figure 1.) show spherical, ~5nm ceria nanoparticles. Based on these results, we determine that the formulations show particles of comparable size morphology, and zeta potential. From here, the ability of each formulation to chemically degrade hydrogen peroxide was

determined via catalase assay.

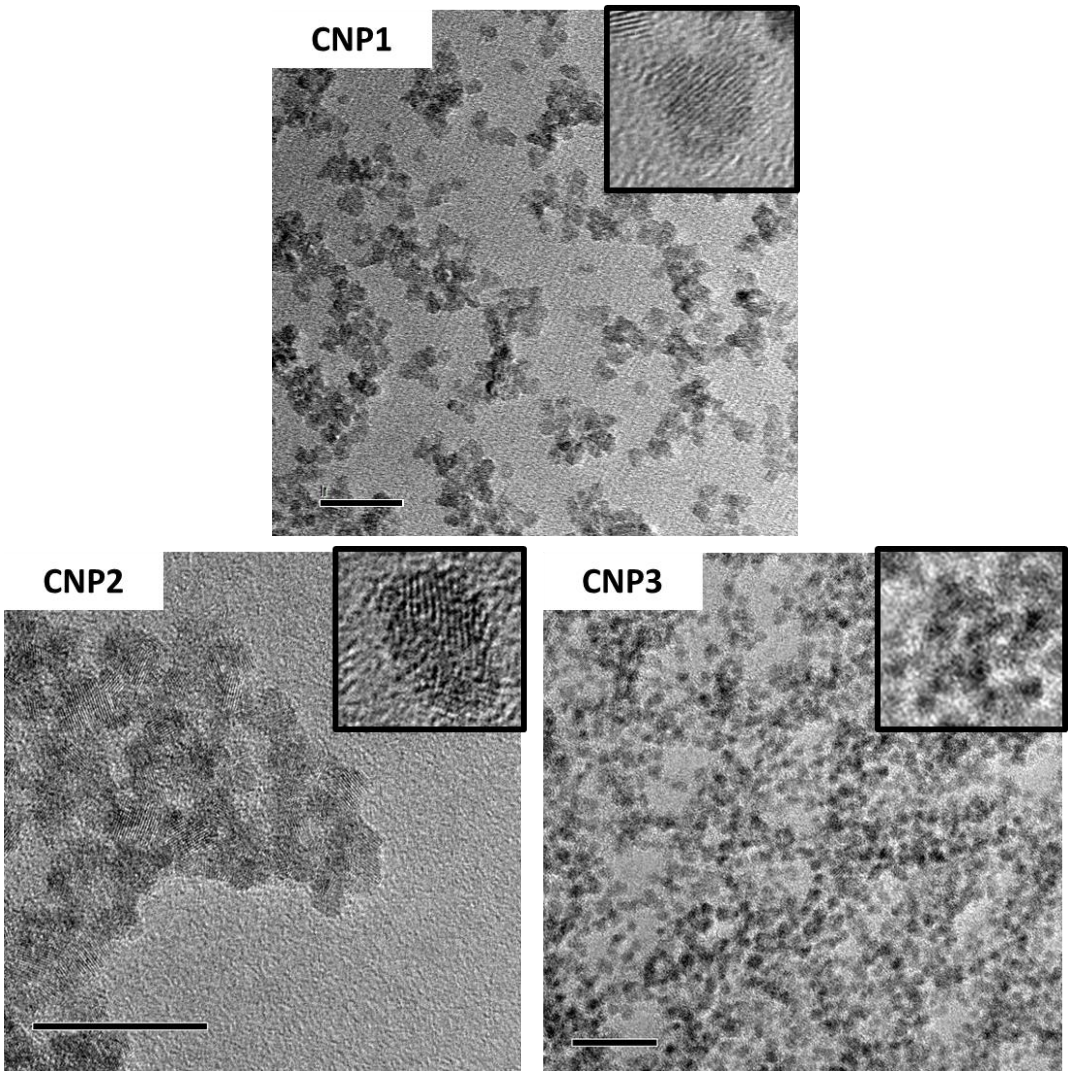

Figure 3 CNP (Left to Right, CNP1,2,3) size Characterization (TEM images) with insets illustrating crystallinity (all scale bars are 20 nm). All formulations show aggregation due to the high reactivity of NP surfaces. Images show well-formed, individual crystallites. Further, these images highlight the crystallinity of these particles through the clear presence of lattice fringes

Catalase assays were conducted across the tested CNP formulations (Figure 2a.) and it was determined that lower Ce^{3+}:Ce^{4+} ratios produced a relative increased catalase activity (i.e.

activity increased from CNP1 → 3) due to the redox conversion of Ce^{4+} → Ce^{3+}, in support of findings from previous studies [2a].

Given that particles from each formulation varied only in Ce^{3+}:Ce^{4+} ratio and that catalase activity was found to vary with this ratio, we next performed electrochemical studies to evaluate whether current response showed a similar relationship.

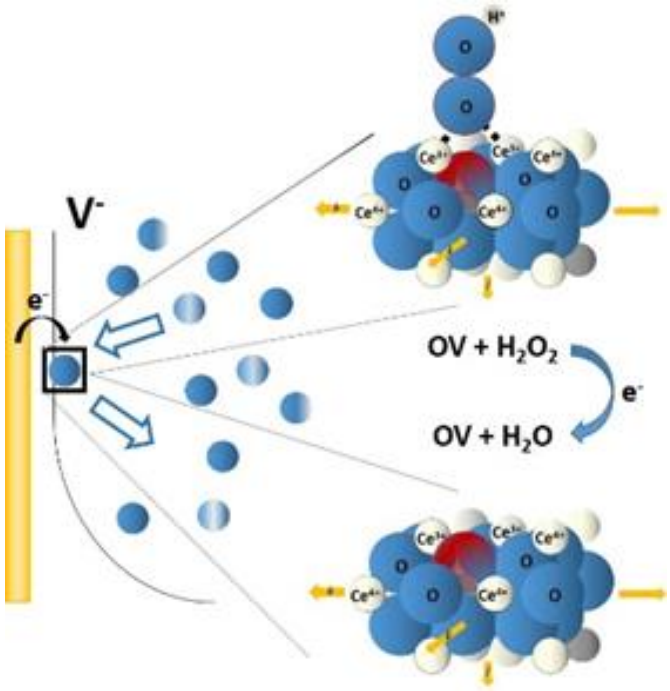

Figure 4 Diagrammatic representation of CNP collision at gold macro-electrode. Collision allows for reduction of adsorbed peroxy species at the working electrode surface and for the re-formation of the ceria surface oxygen vacancies.

3.1 CNPS Electrochemical Characterization

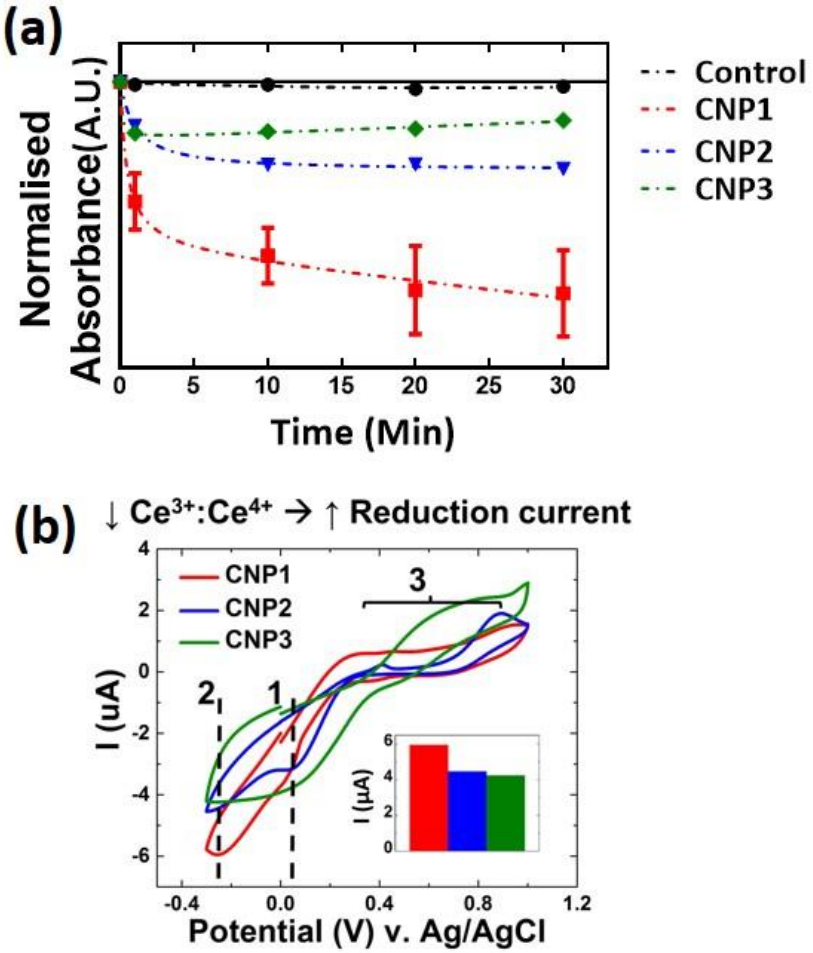

Figure 5 (a) Catalase Assay. Activity was greatest for CNP1 followed in descending order of activity by CNP2 and 3. (b) CV for all CNP preparations (1 mM H_2O_2 and CNPs), cathodic peak current (inset). The inverse relationship between Ce3+:Ce4+ ratio and catalase activity holds for CV. Additionally, an anodic peak present for all formulations shows a positive relationship between Ce^{3+}:Ce^{4+} ratio and current.

Initially, to characterize the electrochemical behavior of each CNP formulation, CV was performed with 1 mM CNPs and 1 mM H_2O_2 for all formulations (Figure 5b.). CV scans were

completely consistent by the third cycle (used for analysis), with subsequent cycles being largely similar (data not shown). Since the current does not change considerably with successive cycles, we determine that the observed current response does not arise from any side reactions in the solutions i.e. not from an ECE-type mechanism wherein an electrochemical change elicits a chemical reaction mediating a current signal[19]. The overall shape of the obtained CV curves were fairly similar across formulations, suggesting similar electrochemical reactions for all formulations [(Allen J. Bard 2001)]. The peaks common to all formulations occur at ~0 V (hereafter, *peak 1*), -0.23 V (*peak 2*) and 0.4-0.7 V (*peak 3*). These are attributed to the CNP-mediated reduction of H_2O_2 (*peaks 1 and 2*) and the oxidation of the Au electrode (*peak 3*) [(Gerlache et al. 1997),(Sardesai et al. 2013)], respectively.

CNPs with lower Ce^{3+}:Ce^{4+} ratio have a more defined peak 1; this has been attributed to the initial reduction of H_2O_2 [(Gerlache et al. 1997)]. In contrast, the higher ratio CNP1 solution shows a more diffuse, wide peak at a similar potential; this behavior is consistent with complex catalysis mechanisms presented in literature [(Sardesai et al. 2013)]. Specifically, the peak character suggests that reduction initially occurs, however, the catalysis is kinetically restricted for high Ce^{3+}:Ce^{4+} formulations. Degradation of H_2O_2, for these formulations occurs very slowly, on the order of days for millimolar concentrations in absence of applied electrical potential [(Neal et al. 2015)]. Additionally, it has been speculated that this diffuse peak represents a multi-step reduction mechanism wherein radical oxygen species (such as superoxide) and/or oxygen are evolved and transiently adsorb at the electrode surface [21]. Peak 2 represents the complete reduction of H_2O_2. This peak is seen to be sharp and intense for lower Ce^{3+}:Ce^{4+} ratio CNP formulations indicative of a fast, diffusion-mediated reduction while higher ratio formulations show a more diffuse peak

which seems to overlap with peak 1 (as detailed above). In similar work [13,(Sardesai et al. 2013)], this cathodic peak was attributed to the CNP-mediated reduction of surface-complexed O_2^{2-}/O_2^- species. The high current increase seen for low ratio formulations was attributed to peroxy-complexed CNPs functioning as nanoelectrodes by colliding with the working electrode and facilitating indirect electron transfers from the working electrode to adsorbed oxygen species [(Rees et al. 2012; Sardesai et al. 2013),(Kahk et al. 2012)]. Particle contact with the conductive electrode resulting in degradation of the surface species occurs primarily through the following relationship,

$$Ce^{4+}{:}H_2O_2 \rightarrow Ce^{3+} + H_2O + O_2 \qquad \text{[(Sardesai et al. 2013)]} \qquad (1)$$

The high current arises from the high surface coverage of the nanoparticles by the peroxy species: allowing reduction of a large quantity of molecules near-simultaneously. In support of this, in a study utilizing CNP collision with microelectrodes, individual CNP impacts were observable with dramatic increases in the current observed for peroxide adsorbed particles relative to CNPs without H_2O_2 exposure[(Sardesai et al. 2013)].

In agreement with catalase data, we observed that lower $Ce^{3+}{:}Ce^{4+}$ ratio formulations produced a nearly two-fold greater cathodic peak current density as compared to higher ratio formulations (determined by normalizing peak currents with respect to electrode electroactive surface area, described in the Experimental section) . Figure 5b details the relative peak current densities for each of the formulations. Lower $Ce^{3+}{:}Ce^{4+}$ ratio better facilitate H_2O_2 reduction based on their oxygen release property. Oxygen release from the CNP lattice is believed to be more favorable for CNPs with higher Ce^{4+} than is for higher Ce^{3+} particles [(Sayle et al. 2005)]. This

may allow for a more favorable reduction reaction by releasing reaction products at a higher rate: explaining the greater cathodic current density for CNP3 over CNP1 as well as the overall shape of the respective CV curves.

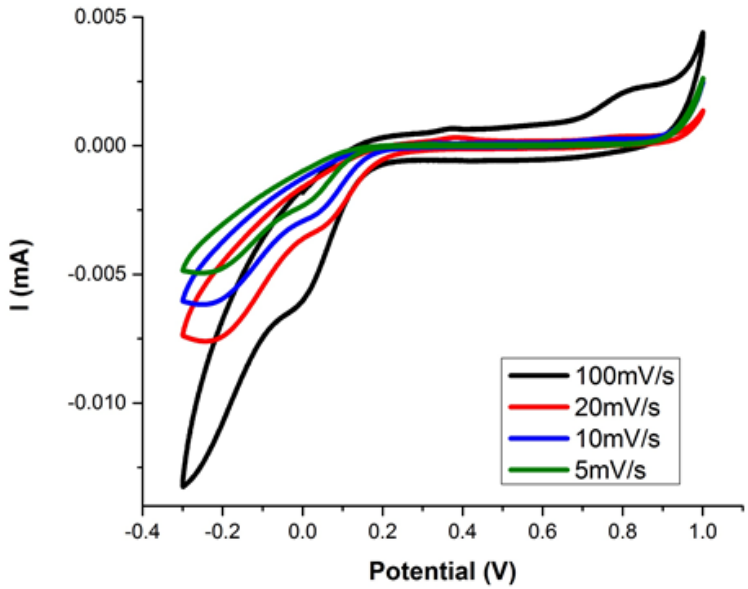

Figure 6 Current Dependence on Scan Rate for CNP-Hydrogen Peroxide reaction at Reduction peak. Linear fitting of the peak reduction current vs. the inverse of scan rate produces an R^2 value of 0.99. This is evidence that the CNP-H_2O_2 reaction is diffusion limited at -0.23V.

Performing CVs at multiple scan rates and plotting the square root of each scan rate vs. the corresponding peak current (Figure 6), we determined that the CNP-mediated peroxide reduction reaction is diffusion-limited [(Allen J. Bard 2001)]. Because the reduction response is produced by nanoparticle flux at the electrode surface, the amperometric signal is dependent on the diffusivity of the nanoparticles, rather than of the peroxide species. This factor is important

in considering the potential response of sensor devices with an adsorbed CNP layer.

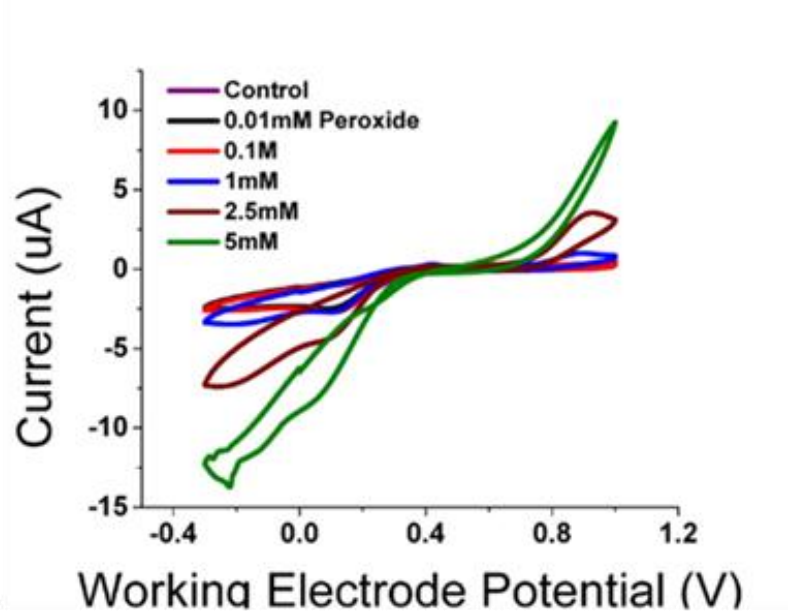

Figure 7 Concentration dependence and peaks character for CNP 1 and 2 formulations. Peaks 1 and 2 show a concentration dependent current response towards hydrogen peroxide. Additionally, the peak at ~0.8V becomes broader- moving towards lower potential values; suggesting a more complex redox mechanism at the electrode.

Additionally, we saw the reverse trend (relative to the trend observed for cathodic current) for anodic current density with higher ratio formulations at peak 3 producing greater current density, similar to literature SOD activity trends[(Pirmohamed et al. 2010)]. This peak was attributed to gold oxidation and has been shown to be sensitive to hydrogen peroxide concentrations [(Gerlache et al. 1997)]. However, no consistent trend with H2O2 concentration was observed for this signal and therefore the signal could not be used for analytical measure. Peak 3 is well-defined and correlates positively with the current density for peroxide reduction at constant peroxide concentration suggesting that hydroxyl species formation is part of the CNP-peroxide reduction mechanism.

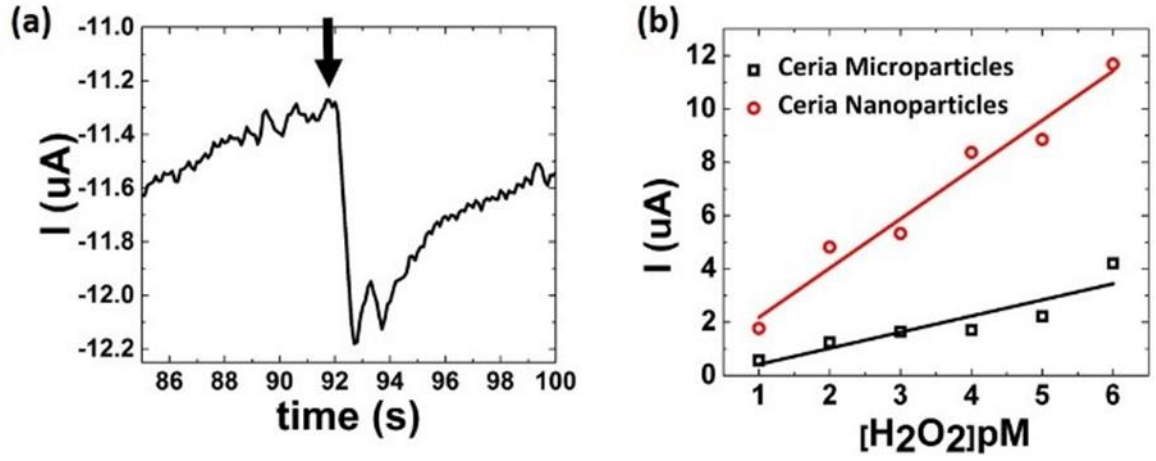

Figure 8 (a) Picomolar detection by Biosensor. Addition of H2O2 to a final concentration of 1pM produces a 350nA signal, compared with the nanomolar limit of detection of most enzymes. (b) Nano v. Micro particle characterization. CNPs show significantly greater sensitivity towards H2O2 analyte as compared to ceria microparticles-based sensor; this greater signal is attributed to nano-size effects and specifically to the change in nanomaterial surface chemistry/physics.

Corroborating this, when another CNP preparation involving a chloride salt pre-cursor does not show this peak at all as a result of strong, preferential Cl^- adsorption at the working electrode surface [M. Gerlache, Z. Senturk, G. Quarin and J.-M. Kauffmann, *Electroanalysis* 1997, *9*, 1088-1092.]. Interestingly, for CNP3, an anodic current begins at 0.4V in the forward scan, however, the peak is considerably more diffuse than is common for the hydroxyl oxidation. Comparing the scan in Figure 5b. with scans of lower concentration hydrogen peroxide (Figure 7), we see that the diffuse peak arises from the convergence of peaks at 0.4 and ~0.8V (this anodic current can thus be decoupled from any background current). This further suggests that lower Ce^{3+}:Ce^{4+} ratio formulations undergo multiple redox reactions involving several oxygen species (based on the substantial peak width

and the presence of multiple peaks at lower peroxide concentrations). The width of this peak in Figure 5b. also suggests a capacitive nature for the species involved (charge development at the working electrode surface from adsorbed oxygen species), further inculpating adsorbed oxygen species. Further, it was concluded in the previously referred study that hydrogen peroxide is more easily oxidized at oxidized gold surfaces.

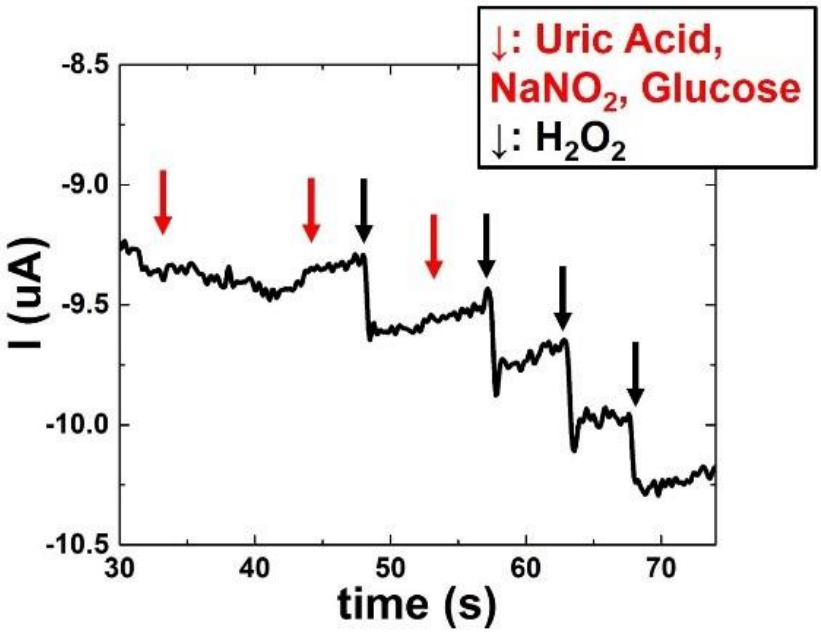

Figure 9 CNP3 CA with addition of Competitive species and H_2O_2. Competitive species addition causes no significant change in current. H_2O_2 addition causes immediate response with each addition.

It was speculated that hydroxyl species at the electrode surface form hydrogen bonds with peroxides allowing for oxidation at lower potentials [M. Gerlache, 1997], in explanation of the convergence of the multiple peaks at low peroxide concentrations to one common peak partway between the constituent peaks. From the present study, we cannot determine conclusively whether

the observed oxidation reaction can be can be ascribed to CNP SOD activity.

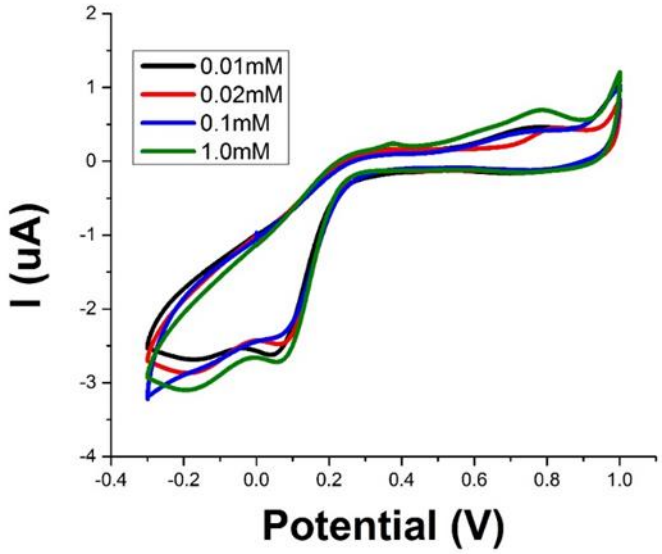

Figure 10 1mM Glucose in dH_2O cyclic voltammogram. Glucose control was run to determine redox interaction with gold. Glucose produces a current response however, the response is not concentration dependent. Therefore, presence of glucose can be disregarded as a background current signal and changes to glucose concentration will not interfere with the sensors current response to hydrogen peroxide analyte.

Due to the strong relationship between Ce^{3+}:Ce^{4+} ratio and cathodic current, we determined to study the CNP-mediated H_2O_2 reduction current response. CA is more suited for quantitative measurements, such as these, over CV [(Allen J. Bard 2001)]. Therefore, the formulations with the least (CNP1) and greatest (CNP3) Ce^{3+}:Ce^{4+} ratio were selected for further investigations to confirm the trends in current values observed in CV and to test the efficacy of the particles as an amperometric assay.CA was performed with several interfering species (shown elsewhere to poison H_2O_2 redox reactions) and with successive additions of 200 uM H_2O_2 to CNP1 and 3

formulations in dH_2O (S4). None of glucose, uric acid, nor sodium nitrite produced any significant current change (Figure 9.) suggesting strong selectivity towards the target analyte. Further, addition of interfering species and H_2O_2 did not produce any measurable response in absence of CNPs (data not shown).

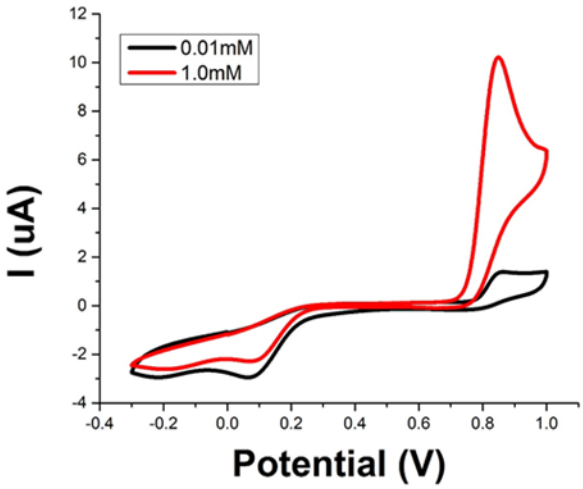

Figure 11 Cyclic voltammagram of Sodium Nitrite in water at 10uM and 1mM. The voltammagram shows little change in current response with concentration of analyte at our determined sensor operating potential, -0.23V.

Upon addition of H_2O_2 to CNP solutions, an immediate current response was observed (Figure 13.). Comparing CA data for CNP1 to CNP3 formulations shows significantly greater (> 125%) current values for CNP3, similar to the differences observed in CV measures (Figure 7). Addition of 200uM (final concentrations) of uric acid, glucose, and sodium nitrite in succession shows no significant response for either solution. Addition of 10uL of 200mM H_2O_2 shows instantaneous amperometric response. (**aii and bii**) Regressions for both formulations show high correlation. Slopes of these lines represent sensitivity of detection with CNP3 having greater

sensitivity. Additionally, with similar concentrations and addition protocols for hydrogen peroxide, varying the concentration of CNPs in solution predictably changed the current output at peak 1 (Data not shown). Redox active species do not produce measurable current at the working electrode in absence of CNPs, interfering species do not interact with hydrogen peroxide to produce CNP-sensitive by-products, and interfering species do not produce a redox reaction with CNPs which could have produced the observed current.

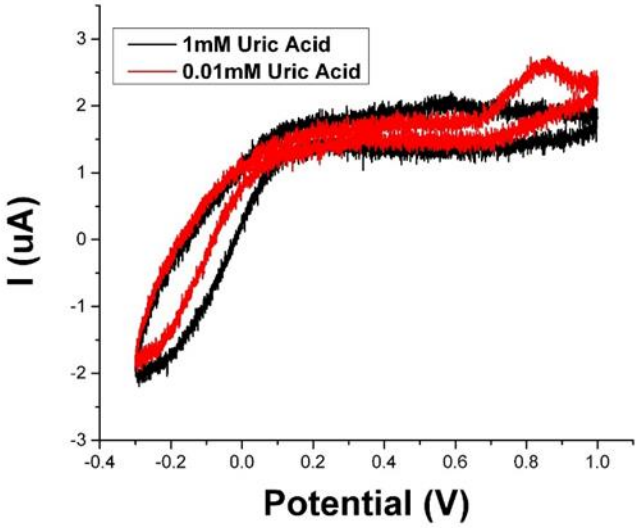

Figure 12 Uric Acid Cyclic Voltammetry interfering species. Voltammetry at 1 and 0.01mM concentrations shows little change in current at the hydrogen peroxide reduction potential. From this, it seems that the sensor will operate independent of uric acid concentration and that presence of uric acid will only contribute to background current.

Based on these results we believe that CNP formulations with lower Ce^{3+}:Ce^{4+} are better suited for amperometric detection of hydrogen peroxide. Further, due to the success of the CNP3

formulation in producing a considerable current, we fabricated a sensor based on immobilizing CNPs on a glassy carbon electrode. The sensor was able to produce signals at the picomolar (parts per trillion) concentration level (Figure 8a.). This level of detection is highly competitive with enzyme-based sensors which typically function in the nanomolar region [(Saha et al. 2009)]. In comparison with CV data, the increased current response likely arises from the proximity of CNPs to the electrode surface. Particle-mediated H_2O_2 reduction is limited by H_2O_2 diffusion to the particle-coated electrode surface, rather than by the CNP diffusion limitation for the solution-based CNP method. Therefore, the electrode experiences a greater flux at its surface immediately following peroxide addition, increasing the achieved signal. To optimize our sensor design and in considering the generally observed trend of increasing ionic diffusion for nanomaterials over micron-scale materials, we sought to characterize the influence of nano-scale chemical properties of the ceria film [(Rivest and Jain 2013), (Rupp 2012)].

To accomplish this, measurements from the sensor described above were compared with those of an analogous sensor based on a CMP film (Figure 8b.). As shown, the CNP-based sensor boasts a significantly greater sensitivity. Ostensibly, the nano- character of the particles allows for more efficient/effective surface catalysis resulting in a greater electrochemical signal. This character has been well-studied in ceria and is often ascribed to the bond strain produced in ceria when reduced to nano-dimensions[(Deshpande et al. 2005b)]. Therefore, the CNP-based sensor platform was further analyzed for detection ability.

CA was performed to determine H_2O_2 detection range for the CNP-based device. It was found that the sensor produced reliable signals across seven orders of magnitude (from 0.1pM to 0.1uM) (Figure 15.). The lower bound of this range was determined using the convention for limit of

quantitation (LOQ); specifically,

$$LOQ = (\text{Root Mean Square of Blank current}) + 10\sigma_{RMS,\ Blank}$$

The obtained range includes concentrations relevant to physiological conditions. Beyond this, the LOQ of this detection range is several orders of magnitude lower than that of enzyme-based devices (nanomolar limits). From here, the sensor platform was tested for robustness in different chemical environments.

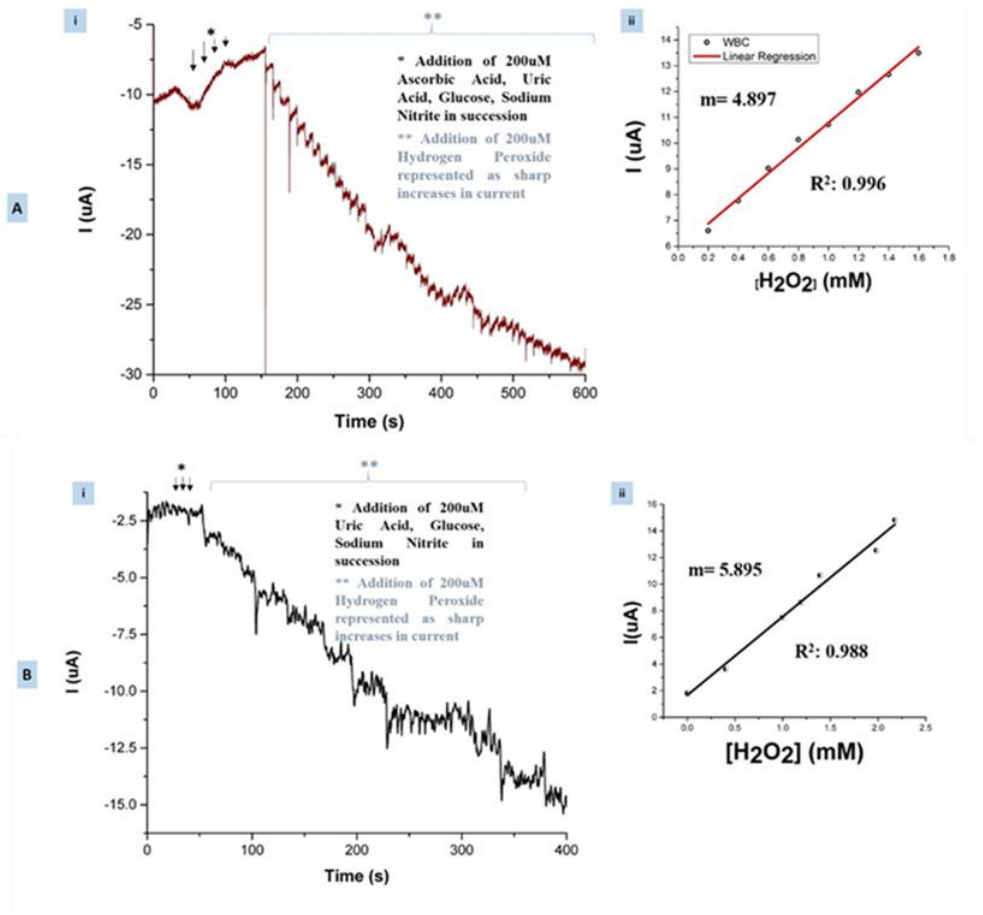

Figure 13 CA (i) of CNPs1 ***(a)*** *& 3* ***(b)*** *in solution with regression for each* ***(ii)****.* ***(ai & bi).*** *Measurements for both formulations show good linear fit between current and* H_2O_2*. Comparison between these two responses corroborates results in CV measurements and allows*

for optimization of the CNP sensing element in biosensor application.

Figure 16a,b. shows that the sensor experiences no loss in activity across the measured pH (4-8) and temperature ranges (20-40^{0}C). Further, as a ceramic material, CNPs exhibit high thermal stability without structure changes well beyond temperatures practical for biosensing[(Murray et al. 1999)]. In order to utilize the sensor platform as a true biosensor: it must be stable against solution leaching and biofouling. The as-synthesized glassy carbon electrodes have a moderately porous structure (Figure 1). We believe that this structure played an important role in maintaining CNP-adsorption on the electrode surface as previous attempts with gold working electrodes used for solution-based CNP electrochemical characterization saw significant CNP layer leeching into test solutions (data not shown). However, the CNP comprised film is still vulnerable to degradation and in bio-solutions the surface can be blocked by adsorbed proteins (bio-fouled) [(Barkam et al. 2013), (Saraf et al. 2015)]. Therefore, we next applied a thin layer of nafion to the sensor and tested in blood serum [(You et al. 2011)].

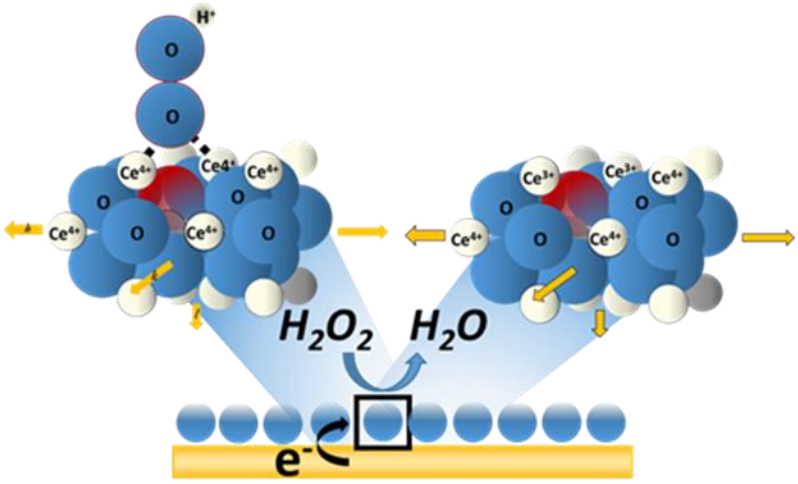

Figure 14 Diagrammatic representation of deposited CNP film on glassy carbon substrate. Particles are located directly on the electrode surface allowing for immediate peroxy species

reduction and for high electron flux due to the fixed position of the CNPs at the electrode surface.

Addition of the nafion film was done to prevent adsorption of protein. However, it is likely that formation of the film would decrease the overall sensitivity of the sensor. Therefore, the nafion-coated sensor was first tested in salt solution rather than in serum to compare with the uncoated sensor. Chronoamperometry showed that the nafion coating had only a moderate influence on current response of the sensor: producing a loss in sensitivity of less than 8% as compared with the non-coated sensor.

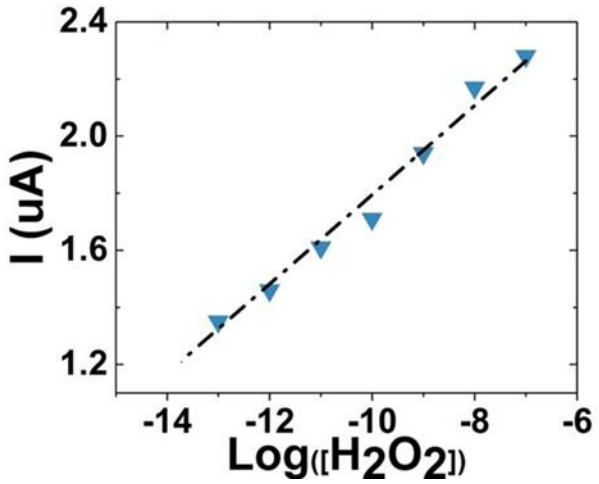

Figure 15 Sensor detection range for H2O2. The detection range is across eight orders of magnitude from 0.1pM to 0.1uM.

CA measurement in blood serum with nafion-coated electrodes showed clear current response upon addition of analyte (Figure 16c.). In contrast, measurements using electrodes without a nafion coating experienced total loss of signal. Since the signal is regained upon addition of the nafion coating, it can be said that the loss in signal is due to solution components

interacting directly with the CNP layer, rather than solely a chemical interaction between the hydrogen peroxide analyte and some solution component. Therefore, loss in signal is likely related to protein adsorption at the electrode surface: preventing the direct interaction of hydrogen peroxide analyte with the electrode surface. Further, incubation of the nafion-coated sensor in serum overnight caused no additional loss in sensitivity indicating resistance to bio-fouling and suggesting that the sensor could potentially be used for in vivo or in vitro conditions.

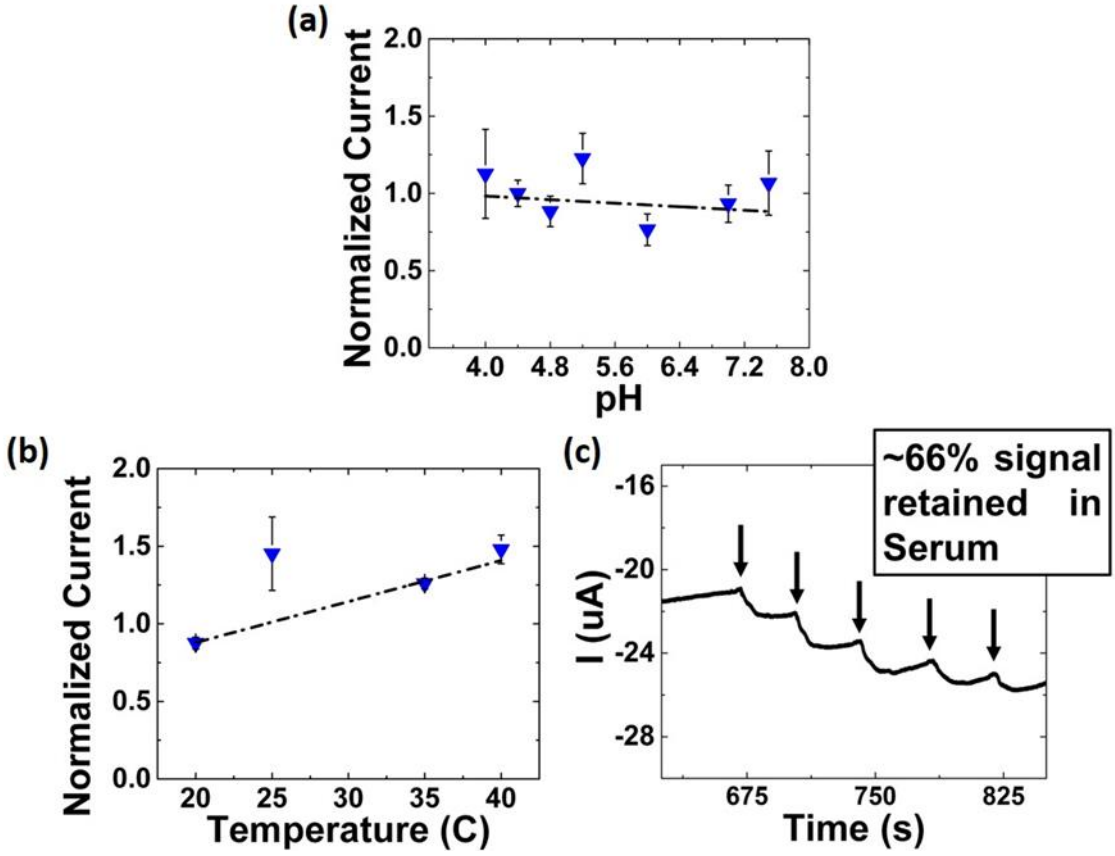

Figure 16 The sensor shows no loss in activity from (a) pH 4.0 to 8.0 or from (b) 20 to 40 ^{o}C , as compared with HRP which loses significant activity across these ranges. Further, experiences a melting point at 42 ^{o}C resulting in loss of tertiary structure. (c) CA with nafion-coated CNP-based sensor in blood serum. Serial additions of 1uM H2O2 produces clear current signal

suggesting absence of bio-fouling.

These results are promising for the potential application of the sensor platform with implantable devices. The sensor could potentially operate as a stand-alone implanted device or could be integrated with other implanted devices to provide specific, real-time information to control some actuating device.

CHAPTER FOUR: CONCLUSION

From this study, a deeper understanding of ceria nanoparticle (CNP) electrochemistry as a function of Ce^{+3}:Ce^{+4} ratio has been developed. We have shown that the trend observed in CNPs' Ce^{3+}:Ce^{4+} ratio for catalase-mimetic degradation of H_2O_2, as extensively studied elsewhere through optical/dye-based assays, extends to electrochemical activity. It is determined that a lower ratio of Ce^{3+}:Ce^{4+} redox states elicits a greater current response towards H_2O_2 than do particle formulations with a greater relative concentration of Ce^{3+}. This understanding is critical to the application of CNPs in catalysis-devices and assays. In this study, this physical-chemical property has been implemented to develop a high sensitivity, high selectivity enzyme-free CNP-based biosensor.

The fabricated biosensor platform with CNPs showed a picomolar range limit of detection while remaining insensitive to interfering species know to undergo electrochemical redox at lower overpotentials (evidencing high selectivity). Additionally, interfering redox species of biological importance were also chosen to better characterize the biosensors potential for functioning in bio-fluids and in vitro/in vivo conditions. Further, the advantage of nano-size effects was seen as greater sensitivity when comparing to an analogous microparticle-based sensor. In this way, choosing to incorporate nanoparticles over a microparticle formulation is another form of optimization for the studied sensor platform.

We have also shown that the sensor platform retains sensitivity across pH and temperature ranges wherein analogous enzymes lose significant activity. In addition, the ceria-based biosensor demonstrated excellent detection of H_2O_2 in blood serum implying potential as a

translational technology to an implanted medical device.

Building from this work, in the future, it will be beneficial to investigate the influence of varying oxygen concentrations on the performance of the sensor. Throughout the body, the cell systems comprising tissues experience different physiological environments including oxygen partial pressure. This physiological condition is especially true, for example in cancer tissues and during ischemic attacks. Being that hydrogen peroxide detecting biosensors will likely be implanted into organs highly susceptible to ischemic conditions (e.g. brain, lungs, heart), the influence of these conditions on sensor signals will be of vital importance. These different magnitudes of oxygen saturation could influence the surface reactivity of the CNPs by lowering the reaction products. Thus, in lower concentrations of environmental oxygen, it may be that the equilibrium concentrations of surface reaction products will be shifted and induce/inhibit the degradation of analytes. This information will be of critical importance when monitoring hypoxic (physiologically low partial pressures of oxygen) conditions. Additionally, in future studies it will be highly beneficial to make a self-contained device package for the produced biosensor platform. By integrating the three electrode electrochemical set up, a power source, and a transmitter, the produced biosensor platform can potentially be of significant use for clinical practices. Further, due to the robustness of the platform (demonstrated in the study as relative pH, temperature, and bio-fouling insensitivity), a self-contained device could open new opportunities for field use. The device could be utilized effectively and reliably across various environmental conditions.

LIST OF REFERENCES

1. Alili, L., Sack, M., Karakoti, A.S., Teuber, S., Puschmann, K., Hirst, S.M., Reilly, C.M., Zanger, K., Stahl, W., Das, S., 2011. Combined cytotoxic and anti-invasive properties of redox-active nanoparticles in tumor–stroma interactions. Biomaterials 32(11), 2918-2929.
2. Allen J. Bard, L.R.F., 2001. Electrochemical Methods: Fundamentals and Applications. Wiley.
3. Ansari, A.A., Kaushik, A., Solanki, P.R., Malhotra, B.D., 2008. Sol–gel derived nanoporous cerium oxide film for application to cholesterol biosensor. Electrochemistry Communications 10(9), 1246-1249.
4. Asati, A., Santra, S., Kaittanis, C., Nath, S., Perez, J.M., 2009. Oxidase Activity of Polymer-Coated Cerium Oxide Nanoparticles. Angewandte Chemie (International ed. in English) 48(13), 2308-2312.
5. Barkam, S., Saraf, S., Seal, S., 2013. Fabricated Micro-Nano Devices for In vivo and In vitro Biomedical Applications. Wiley Interdisciplinary Reviews: Nanomedicine and Nanobiotechnology 5(6), 544-568.
6. Cai, X., Gorbatyuk, M.S., Lewin, A.S., Chen, L., Dong, J., Hauswirth, W.W., Seal, S., McGinnis, J.F., 2014. Nanoceria with Grp78/Bip produce enhanced inhibition of retinal degeneration in tubby mice. Investigative Ophthalmology & Visual Science 55(13), 4622-4622.

7. Chattopadhyay, K., Mazumdar, S., 2000. Structural and Conformational Stability of Horseradish Peroxidase: Effect of Temperature and pH. Biochemistry 39(1), 263-270.
8. Chen, W., Cai, S., Ren, Q.-Q., Wen, W., Zhao, Y.-D., 2012. Recent advances in electrochemical sensing for hydrogen peroxide: a review. Analyst 137(1), 49-58.
9. Das, S., Dowding, J.M., Klump, K.E., McGinnis, J.F., Self, W., Seal, S., 2013. Cerium oxide nanoparticles: applications and prospects in nanomedicine. Nanomedicine 8(9), 1483-1508.
10. Delvaux, M., Walcarius, A., Demoustier-Champagne, S., 2004. Electrocatalytic H2O2 amperometric detection using gold nanotube electrode ensembles. Analytica Chimica Acta 525(2), 221-230.
11. Deshpande, S., Patil, S., Kuchibhatla, S.V., Seal, S., 2005a. Size dependency variation in lattice parameter and valency states in nanocrystalline cerium oxide. Applied Physics Letters 87(13), 133113-133113.
12. Deshpande, S., Patil, S., Kuchibhatla, S.V., Seal, S., 2005b. Size dependency variation in lattice parameter and valency states in nanocrystalline cerium oxide. Applied Physics Letters 87(13), 133113.
13. Dowding, J., Song, W., Bossy, K., Karakoti, A., Kumar, A., Kim, A., Bossy, B., Seal, S., Ellisman, M., Perkins, G., 2014. Cerium oxide nanoparticles protect against Aβ-induced mitochondrial fragmentation and neuronal cell death. Cell Death & Differentiation 21(10), 1622-1632.
14. Dowding, J.M., Dosani, T., Kumar, A., Seal, S., Self, W.T., 2012. Cerium oxide nanoparticles scavenge nitric oxide radical ([radical dot]NO). Chemical Communications

48(40), 4896-4898.

15. Dowding, J.M., Seal, S., Self, W.T., 2013. Cerium oxide nanoparticles accelerate the decay of peroxynitrite (ONOO−). Drug Delivery and Translational Research 3(4), 375-379.
16. Gerlache, M., Senturk, Z., Quarin, G., Kauffmann, J.-M., 1997. Electrochemical behavior of H2O2 on gold. Electroanalysis 9(14), 1088-1092.
17. Gomes, A., Fernandes, E., Lima, J.L.F.C., 2005. Fluorescence probes used for detection of reactive oxygen species. Journal of Biochemical and Biophysical Methods 65(2–3), 45-80.
18. Gupta, A., Das, S., Neal, C.J., Seal, S., 2016. Controlling the surface chemistry of cerium oxide nanoparticles for biological applications. Journal of Materials Chemistry B.
19. Hanaoka, S., Lin, J.-M., Yamada, M., 2001. Chemiluminescent flow sensor for H 2 O 2 based on the decomposition of H 2 O 2 catalyzed by cobalt (II)-ethanolamine complex immobilized on resin. Analytica Chimica Acta 426(1), 57-64.
20. Heckert, E.G., Karakoti, A.S., Seal, S., Self, W.T., 2008. The role of cerium redox state in the SOD mimetic activity of nanoceria. Biomaterials 29(18), 2705-2709.
21. Jana, S.K., Banerjee, P., Das, S., Seal, S., Chaudhury, K., 2014. Redox-active nanoceria depolarize mitochondrial membrane of human colon cancer cells. Journal of nanoparticle research 16(6), 1-9.
22. Kahk, J.M., Rees, N.V., Pillay, J., Tshikhudo, R., Vilakazi, S., Compton, R.G., 2012. Electron transfer kinetics at single nanoparticles. Nano Today 7(3), 174-179.
23. Korsvik, C., Patil, S., Seal, S., Self, W.T., 2007. Superoxide dismutase mimetic properties exhibited by vacancy engineered ceria nanoparticles. Chemical Communications(10), 1056-1058.

24. Long, J.S., Silvester, D.S., Wildgoose, G.G., Surkus, A.-E., Flechsig, G.-U., Compton, R.G., 2008. Direct electrochemistry of horseradish peroxidase immobilized in a chitosan–[C4mim][BF4] film: Determination of electrode kinetic parameters. Bioelectrochemistry 74(1), 183-187.
25. McGinnis, J.F., Chen, J., Wong, L., Sezate, S., Seal, S., Patil, S., 2010. Inhibition of reactive oxygen species and protection of mammalian cells. Google Patents.
26. Murray, E.P., Tsai, T., Barnett, S.A., 1999. A direct-methane fuel cell with a ceria-based anode. Nature 400(6745), 649-651.
27. Neal, C.J., Das, S., Saraf, S., Tetard, L., Seal, S., 2015. Self-Assembly of PEG-Coated Ceria Nanoparticles Shows Dependence on PEG Molecular Weight and Ageing. ChemPlusChem 80(11), 1680-1690.
28. Nogueira, R.F.P., Oliveira, M.C., Paterlini, W.C., 2005. Simple and fast spectrophotometric determination of H2O2 in photo-Fenton reactions using metavanadate. Talanta 66(1), 86-91.
29. Pirmohamed, T., Dowding, J.M., Singh, S., Wasserman, B., Heckert, E., Karakoti, A.S., King, J.E.S., Seal, S., Self, W.T., 2010. Nanoceria exhibit redox state-dependent catalase mimetic activity. Chemical communications (Cambridge, England) 46(16), 2736-2738.
30. Qu, F., Yang, M., Shen, G., Yu, R., 2007. Electrochemical biosensing utilizing synergic action of carbon nanotubes and platinum nanowires prepared by template synthesis. Biosensors and Bioelectronics 22(8), 1749-1755.
31. Rees, N.V., Zhou, Y.-G., Compton, R.G., 2012. Making contact: charge transfer during particle-electrode collisions. RSC Advances 2(2), 379-384.

32. Reichert, J.S., McNeight, S.A., Rudel, H.W., 1939. Determination of Hydrogen Peroxide and Some Related Peroxygen Compounds. Industrial & Engineering Chemistry Analytical Edition 11(4), 194-197.
33. Rivest, J.B., Jain, P.K., 2013. Cation exchange on the nanoscale: an emerging technique for new material synthesis, device fabrication, and chemical sensing. Chemical Society Reviews 42(1), 89-96.
34. Rupp, J.L., 2012. Ionic diffusion as a matter of lattice-strain for electroceramic thin films. Solid State Ionics 207, 1-13.
35. Sack, M., Alili, L., Karaman, E., Das, S., Gupta, A., Seal, S., Brenneisen, P., 2014. Combination of conventional chemotherapeutics with redox-active cerium oxide nanoparticles—a novel aspect in cancer therapy. Molecular cancer therapeutics 13(7), 1740-1749.
36. Saha, S., Arya, S.K., Singh, S.P., Sreenivas, K., Malhotra, B.D., Gupta, V., 2009. Nanoporous cerium oxide thin film for glucose biosensor. Biosensors and Bioelectronics 24(7), 2040-2045.
37. Saraf, S., Neal, C.J., Park, S., Das, S., Barkam, S., Cho, H.J., Seal, S., 2015. Electrochemical study of nanoporous gold revealing anti-biofouling properties. RSC Advances 5(58), 46501-46508.
38. Sardesai, N.P., Andreescu, D., Andreescu, S., 2013. Electroanalytical Evaluation of Antioxidant Activity of Cerium Oxide Nanoparticles by Nanoparticle Collisions at Microelectrodes. Journal of the American Chemical Society 135(45), 16770-16773.
39. Sayle, T.X., Parker, S.C., Sayle, D.C., 2005. Phys. Chem. Chem. Phys. 7(15), 2936.

40. Seal, S., Cho, H., Patil, S., Mehta, A., 2012. Cerium oxide nanoparticle regenerative free radical sensor. Google Patents.
41. Self, W.T., Bossy-wetzel, E., Seal, S., Dowding, J., 2016. NEURONAL PROTECTION BY CERIUM OXIDE NANOPARTICLES. US Patent 20,160,038,537.
42. Tarnuzzer, R.W., Colon, J., Patil, S., Seal, S., 2005. Vacancy engineered ceria nanostructures for protection from radiation-induced cellular damage. Nano letters 5(12), 2573-2577.
43. Temoçin, Z., Yiğitoğlu, M., 2008. Studies on the activity and stability of immobilized horseradish peroxidase on poly(ethylene terephthalate) grafted acrylamide fiber. Bioprocess and Biosystems Engineering 32(4), 467-474.
44. Walkey, C., Das, S., Seal, S., Erlichman, J., Heckman, K., Ghibelli, L., Traversa, E., McGinnis, J.F., Self, W.T., 2015. Catalytic properties and biomedical applications of cerium oxide nanoparticles. Environmental Science: Nano 2(1), 33-53.
45. Wang, J., 2006. Electrochemical biosensors: Towards point-of-care cancer diagnostics. Biosensors and Bioelectronics 21(10), 1887-1892.
46. Wason, M.S., Colon, J., Das, S., Seal, S., Turkson, J., Zhao, J., Baker, C.H., 2013. Sensitization of pancreatic cancer cells to radiation by cerium oxide nanoparticle-induced ROS production. Nanomedicine: Nanotechnology, Biology and Medicine 9(4), 558-569.
47. Xu, Y., Peng, W., Liu, X., Li, G., 2004. A new film for the fabrication of an unmediated H2O2 biosensor. Biosensors and Bioelectronics 20(3), 533-537.
48. You, J.-M., Jeong, Y.N., Ahmed, M.S., Kim, S.K., Choi, H.C., Jeon, S., 2011. Reductive determination of hydrogen peroxide with MWCNTs-Pd nanoparticles on a modified glassy

carbon electrode. Biosensors and Bioelectronics 26(5), 2287-2291.

49. Zhao, J., Zhang, Y., Li, H., Wen, Y., Fan, X., Lin, F., Tan, L., Yao, S., 2011. Ultrasensitive electrochemical aptasensor for thrombin based on the amplification of aptamer–AuNPs–HRP conjugates. Biosensors and Bioelectronics 26(5), 2297-2303.